ACS Sustainable Chemistry & Engineering

Subscriber access provided by INDIAN INST OF TECH KHARAGPUR

Article

Electroreduction of carbon dioxide into selective hydrocarbon at low overpotential using isomorphic atomic substitution in copper oxide

Subramanian Nellaiappan, Ritesh Kumar, C. Shivakumara, Silvia Irusta, Jordan A. Hachtel, Juan Carlos Idrobo, Abhishek K. Singh, Chandra Sekhar Tiwary, and Sudhanshu Sharma

ACS Sustainable Chem. Eng., **Just Accepted Manuscript** • DOI: 10.1021/acssuschemeng.9b05087 • Publication Date (Web): 22 Nov 2019

Downloaded from pubs.acs.org on November 27, 2019

Just Accepted

"Just Accepted" manuscripts have been peer-reviewed and accepted for publication. They are posted online prior to technical editing, formatting for publication and author proofing. The American Chemical Society provides "Just Accepted" as a service to the research community to expedite the dissemination of scientific material as soon as possible after acceptance. "Just Accepted" manuscripts appear in full in PDF format accompanied by an HTML abstract. "Just Accepted" manuscripts have been fully peer reviewed, but should not be considered the official version of record. They are citable by the Digital Object Identifier (DOI®). "Just Accepted" is an optional service offered to authors. Therefore, the "Just Accepted" Web site may not include all articles that will be published in the journal. After a manuscript is technically edited and formatted, it will be removed from the "Just Accepted" Web site and published as an ASAP article. Note that technical editing may introduce minor changes to the manuscript text and/or graphics which could affect content, and all legal disclaimers and ethical guidelines that apply to the journal pertain. ACS cannot be held responsible for errors or consequences arising from the use of information contained in these "Just Accepted" manuscripts.

is published by the American Chemical Society. 1155 Sixteenth Street N.W., Washington, DC 20036

Published by American Chemical Society. Copyright © American Chemical Society. However, no copyright claim is made to original U.S. Government works, or works produced by employees of any Commonwealth realm Crown government in the course of their duties.

Electroreduction of Carbon Dioxide into Selective Hydrocarbon at Low Overpotential Using Isomorphic Atomic Substitution in Copper Oxide

Subramanian Nellaiappan[†], Ritesh Kumar[ζ], C. Shivakumara[‡], Silvia Irusta[§], Jordan A. Hachtel[ϒ], Juan-Carlos Idrobo[ϒ], Abhishek K. Singh[ζ], Chandra Sekhar Tiwary[ψ], Sudhanshu Sharma[†]*

[†]Department of Chemistry, Indian Institute of Technology Gandhinagar, Palaj, Gandhinagar 382355, Gujarat, India
[ζ]Materials Research center, Indian Institute of Science, Bangalore-560012, India
[‡]Solid State and Structural Chemistry Unit, Indian Institute of Science, Bangalore 560012, India
[§]Department of Chemical Engineering, Nanoscience Institute of Aragon (INA), University of Zaragoza, 50018 Zaragoza, Spain
[ϒ] Center for Nanophase Materials Sciences, Oak Ridge National Laboratory, Oak Ridge, Tennessee, USA
[ψ]Metallurgical and Materials Engineering, Indian Institute of Technology, Kharagpur, India

*Corresponding Author E-mail: ssharma@iitgn.ac.in (S.S), chandra.tiwary@metal.iitkgp.ac.in (C.S.T), abhishek@iisc.ac.in (A.K.S)

ABSTRACT

The conversion of carbon dioxide into selective hydrocarbons is vital for green energy generation. Due to the chemical instability and lower activity, environmentally stable transition metal oxides (e.g. CuO) are unpopular for CO_2 electroreduction catalysis. Here, we demonstrate substitution of Cu with isomorphic atom i.e. Ni in the CuO and utilize it for improving the hydrocarbon selectivity by 4 times as compared to pristine CuO. Hydrocarbon formation is achieved at the lowest possible applied potential (-0.2 V RHE). This gives the overpotential of about 0.37 V for methane and 0.28 V for ethylene, the lowest ever reported. Employing the ionic interaction between Ni and Cu, this catalyst suppresses the hydrogen evolution reaction (HER) to improve the hydrocarbon selectivity prominently. It is observed that current normalized by the BET surface area gives 15 to 20 times enhancement in the case of Ni substituted CuO compared to undoped CuO. The *in situ* experiments indicate that Ni doped CuO prefers CO pathways compared to formate resulting into high hydrocarbon selectivity. The experimental observation is further supported by DFT studies, which reveals that Ni-doped CuO catalyst has higher limiting potential for CO_2 electro-reduction to CH_4 due to the stabilization of CH_2O intermediate on $Cu_{0.9375}Ni_{0.0625}O$ surface rather than the CHO intermediate, in comparison to the pristine CuO surface.

KEYWORDS: redox-active catalyst, isomorphic atomic substitution, nickel-substituted copper oxide, CO_2 electroreduction, FTIR and DFT studies.

INTRODUCTION

Conversion of CO_2 in to value added products is beneficial for both environment and energy.[1-2] Alongside thermocatalytic[3] and photochemical[4-5], electrochemical conversion of CO_2 has attracted much interest due to its efficient production of a variety of gaseous and liquid products under ambient temperature and pressure.[2, 6-7] Among these numerous products, C_1- and C_2-hydrocarbons (CH_4 and C_2H_4) are exceptionally attractive but remains elusive due to their high energy densities. In particular, ethylene is highly valuable as it is a key material for manufacturing of polyethylene.[8] There are many challenges associated with the electrochemical reduction of CO_2 such as large overpotential and unavoidable competition with hydrogen evolution reactions (HER) in aqueous environment.[9]

Considerable effort has been devoted to develop new catalyst, which can promote CO_2 electroreduction activity with high efficiency and selectivity while suppressing the competing HER. Several heterogeneous catalysts have been developed to improve the electrocatalytic activity by modifying the bulk surface to nanostructures focusing on Cu,[10-13] Ni,[14] Au,[15] Ag,[16] Sn,[17] In,[18] Pd[19]. Out of these, Cu is unique as being the only material to convert CO_2 into hydrocarbons with high faradaic efficiency[10-13] but it has high overpotential, wide product distribution and undesired hydrogen evolution reaction. To overcome these challenges, alloying Cu with other metals[20-24] and several nano-structured metal oxides[25-28] and derived-metal oxides[29-31] and supported-metal oxides[32-34] have been employed as precursors and/or electrocatalysts for enhanced electrochemical reduction of CO_2 in to desired products. The reasons behind the catalytic activities of these oxides are optimum binding energy of reaction intermediates[25-28], multiple valences metal,[29-31] and synergetic effect.[32-34]

It is well-known that replacing a small fraction of the isomorphic cations in a host metal oxide with a different cations (doping) can change the electrochemical performance of the metal oxide catalyst due to its synergetic effect.[35,36] Adopting the similar substitutional chemistry, we developed a new electrocatalyst by substitution of isomorphic Nickel (Ni^{2+} cation; as dopant) on copper (II) oxide (CuO as host) using solution combustion method. Nickel and Copper in their metallic state have highly similar over potentials for CO_2 electroreduction therefore, it is expected that synergy between the two in the ionic state can tune the electrocatalytic activity. By exploiting the efficient ionic interaction between Cu and Ni, we effectively enhance both CO_2 electroreduction and the hydrocarbon selectivity. This is a new strategy and has not been explored previously.

EXPERIMENTAL SECTION

Synthesis

Solution combustion method has been widely known for preparing the doped metal oxides and simple metal oxides because of its rapidness and large yield of the final product with high crystallinity. In a typical preparation of Ni-doped CuO ($Cu_{1-x}Ni_xO$; x= 0.05 and 0.1), 2.57 g (x=0.05) or 2.72 g (x=0.1) of oxalyldihydrazide (ODH) was dissolved in hot deionized water. This is followed by the addition of 5.0 g of $Cu(NO_3)_2{\cdot}3H_2O$ (99.9% purity) and 0.32 g (x=0.05) or 0.67 g (x=0.1) of $Ni(NO_3)_2{\cdot}6H_2O$ (99.9% purity) to make a clear solution. For CuO, 2.44 g of ODH and 5.0 g of $Cu(NO_3)_2{\cdot}3H_2O$ was used. For NiO, 2.03 g ODH and 5.0 g of $Ni(NO_3)_2{\cdot}6H_2O$ was used. Further, the solution was stirred using glass rod and evaporated by heating at 70°C until we get a homogeneous solution. The as-prepared clear solution was placed in a muffle furnace preheated at 400°C for 20 min. Then, the dish was cooled and powder was collected in crucible, which was kept for calcination at 500 °C for 10 h (Figure 1a). For NiO-deposited-CuO

(NiO/CuO) 200 mg of as-prepared CuO and 73.5 mg $NiNO_3.6H_2O$ (equivalent to 10% Ni in $Cu_{0.9}Ni_{0.1}O$) are dispersed in 10 ml Millipore water followed by sonication for 30 mins. Further, 2 mL of 1.0 M KOH was added drop wise until precipitation starts followed by leaving it for 1 hr. The precipitate was washed thoroughly with water, filtered and dried at 80°C. A final calcination step was carried out at 350°C for 10 hour to convert nickel hydroxide into nickel oxide. Likewise, Ni-deposited-CuO (Ni/CuO) was synthesized by chemical reduction method. Briefly, 200 mg of as-prepared CuO with 73.5 mg $NiNO_3.6H_2O$ (equivalent to 10% Ni in $Cu_{0.9}Ni_{0.1}O$) was dispersed in 10 mL Millipore water. 1 mL of 99% hydrazine hydrate solution was then added drop wise to reduce nickel nitrate into nickel metal. The obtained compound was washed, filtered and kept for drying at 80°C for 4 hrs.

Instrumentation

Combustion synthesized Ni-doped-CuO ($Cu_{0.9}Ni_{0.1}O$, and $Cu_{0.95}Ni_{0.05}O$) and CuO have characterized by powder X-ray diffraction (XRD), Rietveld refinement, BET surface area measurement, field emission scanning electron microscopy (FESEM-EDS), high resolution transmission electron microscopy (HRTEM-EDS), and X-ray photoelectron spectroscopy (XPS). Powder XRD was carried out using Bruker D8 Discover diffractometer (Germany) in the range of 20 − 80° to the crystal phases. The Rietveld refinement was done using the FullProf-fp2k program varying 17 parameters simultaneously such as overall scale factor and background parameter. BET was carried out in Micrometrics 3Flex. Samples were degassed under vacuum at 150°C before the analysis. High resolution scanning electron microscopy was performed by using JEOL (JSM7600F) with energy dispersive spectroscopy (Oxford, Model INCA Energy 250 EDS). The high resolution transmission electron micrographs were acquired using an FEI Titan Themis (s) transmission electron microscope. The XPS was performed with Axis Ultra DLD

(Kratos Analytical Limited). The spectra were obtained by using the mono-chromatized AlKα source (1486.6 eV) run at 15 kV and 10 mA. For the individual peak regions, pass energy of 20 eV was used. Survey spectrum was measured at 160 eV pass energy. Analysis of the peaks was performed with the Casa XPS software, using a weighted sum of Lorentzian and Gaussian components curves after Shirley background subtraction. The binding energies were referenced to the internal C (1s) (284.9 eV) standard.

Electrochemical studies and product analysis

Electrochemical studies were performed using the conventional three-electrode system at CHI660E electrochemical workstation. All solutions were prepared using double-distilled water. Working electrode was made by mixing 100 mg of prepared catalyst and 200 μL of 5% Nafion solution as binder. After that 300 μL of isopropanol was added to it to make thin slurry followed by deposition on a glassy carbon working electrode (GCE). Geometric area of the electrode was 0.071 cm^2. Platinum wire was used as the counter electrode, and Ag/AgCl (saturated KCl) electrode was used as the reference electrode and 0.5M $NaHCO_3$ was used as supporting electrolyte. The estimated uncompensated resistance in the cell is 134.1 ohm. The conversion of potential to RHE was calculated by using the equation: E (RHE) = E (Ag/AgCl) + (0.196 + 0.059 pH). Electroreduction of CO_2 measurements were carried out using the CO_2 saturated 0.5 M $NaHCO_3$ (pH= 6.8) electrolyte, i.e., after CO_2 purging for 30 minutes under room temperature.

An air-tight electrochemical cell was used for the gaseous product formation and analysis. For quantification of gaseous products, a gas-tight syringe (Hamilton, 1000μL) was used to transfer the evolved gases into a gas chromatograph (GC; CIC Baroda). Haysep-A column was used for separation and a Flame Ionization Detector (FID) for detection of CO and hydrocarbons. Thermal Conductivity Detector (TCD) for H_2 detection. A standard gas mixture

was used for calibrating the GC. For liquid products, Gas chromatograph (Agilent 7890) was used.

The faradaic efficiency (FE %) is calculated based on the equation (1):

$$FE\% = \frac{n \times F \times N}{Q} \times 100 \qquad --- \qquad (1)$$

where, n is the number of electron transferred in the faradaic process; F is Faraday constant, 96485 C/mol; N is the amount of the generated product in this process; Q is the total charge passed through the whole reaction.

In situ FTIR under gaseous environment

DRIFTS experiments were performed with CuO and $Cu_{0.9}Ni_{0.1}O$ (mixture of KBr) under different gaseous composition and at different temperatures using a Thermo Scientific NICOLET-iS50 FTIR spectroscope. The DRIFTS cell (Pike Technologies, USA) with an environmental chamber was used to record the IR spectra. The cell was first purged with ultra-high purity nitrogen (UHP N_2). All the experiments were carried out a fixed flow rate of 20 ml min^{-1}, which is controlled by mass flow controller. The catalysts were first heated from room temperature to 200°C and then cooled to room temperature in UHP N_2. FTIR spectra were then recorded at different temperatures in the presence of different gases. A spectrum of powdered KBr recorded in UHP N_2 at room temperature and 100°C which served as the background at room temperature and higher temperatures.

Computational Methodology

Density functional theory (DFT) was used for theoretical calculations, implemented in the Vienna ab initio simulation (VASP) package.[37] Dudarev's approach was utilized for treating the localized nature of electrons in the d orbitals of transition metal oxides.[38] The Electron-ion interactions were described using all-electron projector augmented wave pseudopotentials, and

Perdew-Burke-Ernzerhof (PBE) generalized gradient approximation (GGA)[39] was used to approximate electronic exchange and correlations. The Brillouin zone was sampled using a 10x12x8 and 5x4x1 Monkhorst-Pack k-grid for the bulk and slab calculations, respectively. All structures were relaxed using a conjugate gradient scheme until the energies and each component of the forces converged to 10^{-5} eV and 0.01 eV $Å^{-1}$, respectively. The (111) surface of CuO was generated from their optimized bulk structures using Virtual Nano Lab version 2016.2. The structure of $Cu_{0.9375}Ni_{0.0625}O$ random alloy was generated from CuO (111) surface using the Alloy Theoretic Automated Toolkit (ATAT) code.[40] The structure had 4 layers of atoms with the bottom three layers frozen, and allowing only the topmost layer to relax, in order to mimic the bulk behaviour. For both Cu and Ni atoms, the values of U (Hubbard parameter) and J (on-site Coulomb interaction) were taken to be 7.5 and 1, respectively. The vibrational frequencies were calculated by employing density functional perturbation theory (DFPT).

RESULTS AND DISCUSSION

Characterizations

Figure 1(b) showed the comparative powder X-ray diffraction patterns of $Cu_{0.9}Ni_{0.1}O$, $Cu_{0.95}Ni_{0.05}O$, CuO and NiO. Intense and sharp peaks suggesting that the obtained electrocatalysts are crystalline. In the case of $Cu_{0.95}Ni_{0.05}O$, no additional significant peak corresponding to Ni metal or NiO is observed confirming the substitution of Ni in host CuO and forming solid solution. XRD of $Cu_{0.9}Ni_{0.1}O$ shows two additional new peaks related to NiO, indicating a phase like NiO/$Cu_{1-x}Ni_xO$ forms. Presence of some metallic Ni can also not be ruled out which may be present in low concentration with size in nano range, not detectable in the XRD. XRD of Ni/CuO and NiO/CuO can be seen in Figure S1(a) in supporting information. Both Ni/CuO and NiO/CuO show peaks related to Ni metal and nickel oxide and these are

considered as the supported catalysts. Rietveld refinement is carried out to estimate the correctness of the phase and change in the lattice parameter/volume after the doping. Figure S1(b-d) displayed the observed, calculated and difference plot for $Cu_{0.9}Ni_{0.1}O$, $Cu_{0.95}Ni_{0.05}O$ and CuO, respectively. Rietveld refined plot of $Cu_{0.95}Ni_{0.05}O$ shows closeness between calculated and observed pattern. All the parameters estimated after Reitveld refinements are shown in Supporting Table S1. Considerable decrease in the lattice parameter of CuO after the Ni doping is observed. This agrees with the smaller size of Ni^{2+} ion than Cu^{2+} ion. As a result of decrease in the lattice parameter, there is a decrease in the total lattice volume confirming the bulk doping of Ni^{2+} in CuO host. Lattice shrinking will also have contribution from lattice strain and defects also which will prevent to validate Vegard's law. Surface areas of all the samples are measured by BET method and the surface are values are 0.58 m^2/g, 0.74 m^2/g and 1.7 m^2/g for $Cu_{0.95}Ni_{0.05}O$, $Cu_{0.9}Ni_{0.1}O$, CuO respectively. The surface area for both NiO/CuO and Ni/CuO is 5.0 m^2/g.

Surface morphology and composition of $Cu_{0.9}Ni_{0.1}O$is studied using FE-SEM and HR-TEM with EDS mapping. The FE-SEM along with EDS elemental mapping images of $Cu_{0.9}Ni_{0.1}O$ (Figure 1(c-g)), which confirms the presence of Ni over CuO host. In addition, the dark field TEM image (Figure 2a) and high resolution scanning transmission electron microscopy (STEM) image (Figure 2(b,c)) indicates the cluster nature of $Cu_{0.9}Ni_{0.1}O$. Electron energy-loss spectra (EELS) are acquired from three individual nanoparticles (indicated in Figure 2(c)) that show prominent signals from both the Ni and Cu M-Edges at 68 eV and 74 eV respectively (Figure 2(d)). The composition of the large cluster shown in Figure 2(b) is established through EEL-spectrum imaging, where spectra are acquired at each position in the region of interest. The spatial distributions of the Ni and Cu are shown in Figure 2(e) and 2(f) respectively, with the overlay of the two signals plotted in Figure 2(g). The spectrum imaging

confirms the purity of the catalyst, being composed mostly of Cu with small fractions of Ni. High resolution planar TEM image of $Cu_{0.9}Ni_{0.1}O$ show uniform arrangements of atoms and well-defined lattice fringes with its Fourier transform in the inset (Figure 2(h)) confirming the crystallinity with an inter-planar distance of 0.2 nm and (102) planes. We do observe other binding state of Cu and Ni, which can be attributed to Surface Ni/Cu atoms, vacancy and defects present in samples. Such Ni and Cu atoms may also contribute in chemical reactions as a minor contributor. The above composition studies confirm the presence of Ni, Cu and Ni-substituted-Cu homogeneous regions of $Cu_{0.9}Ni_{0.1}O$.

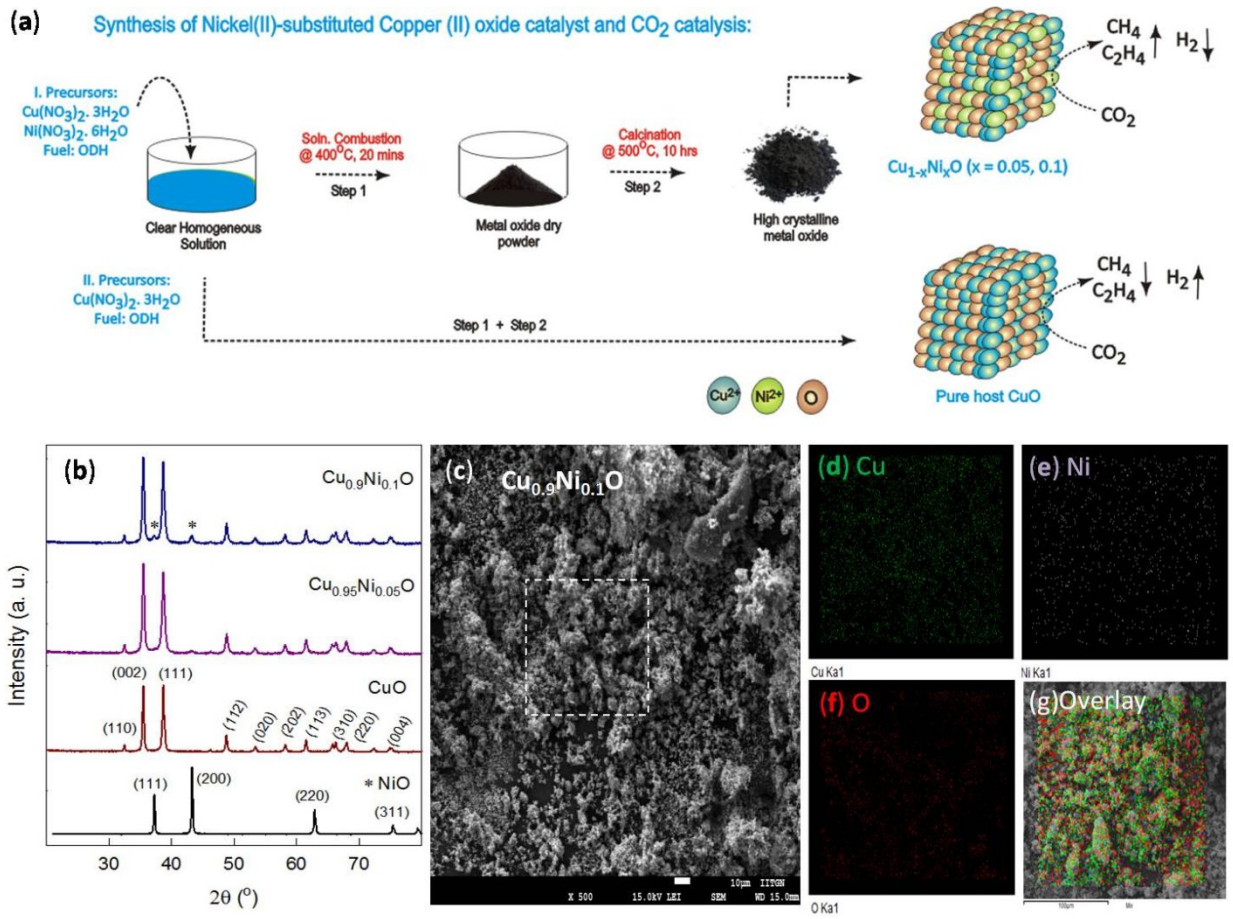

Figure 1. Schematic representation for the synthesis of Ni-substituted-CuO and pure host CuO catalysts using solution combustion method (a), comparative XRD patterns of $Cu_{0.9}Ni_{0.1}O$,

$Cu_{0.95}Ni_{0.05}O$, CuO and NiO catalysts (b), FE-SEM image of $Cu_{0.9}Ni_{0.1}O$ (c) along with EDS elemental mapping for Cu Kα (d), Ni Kα (e), O Kα (f) and its overlay (g) images.

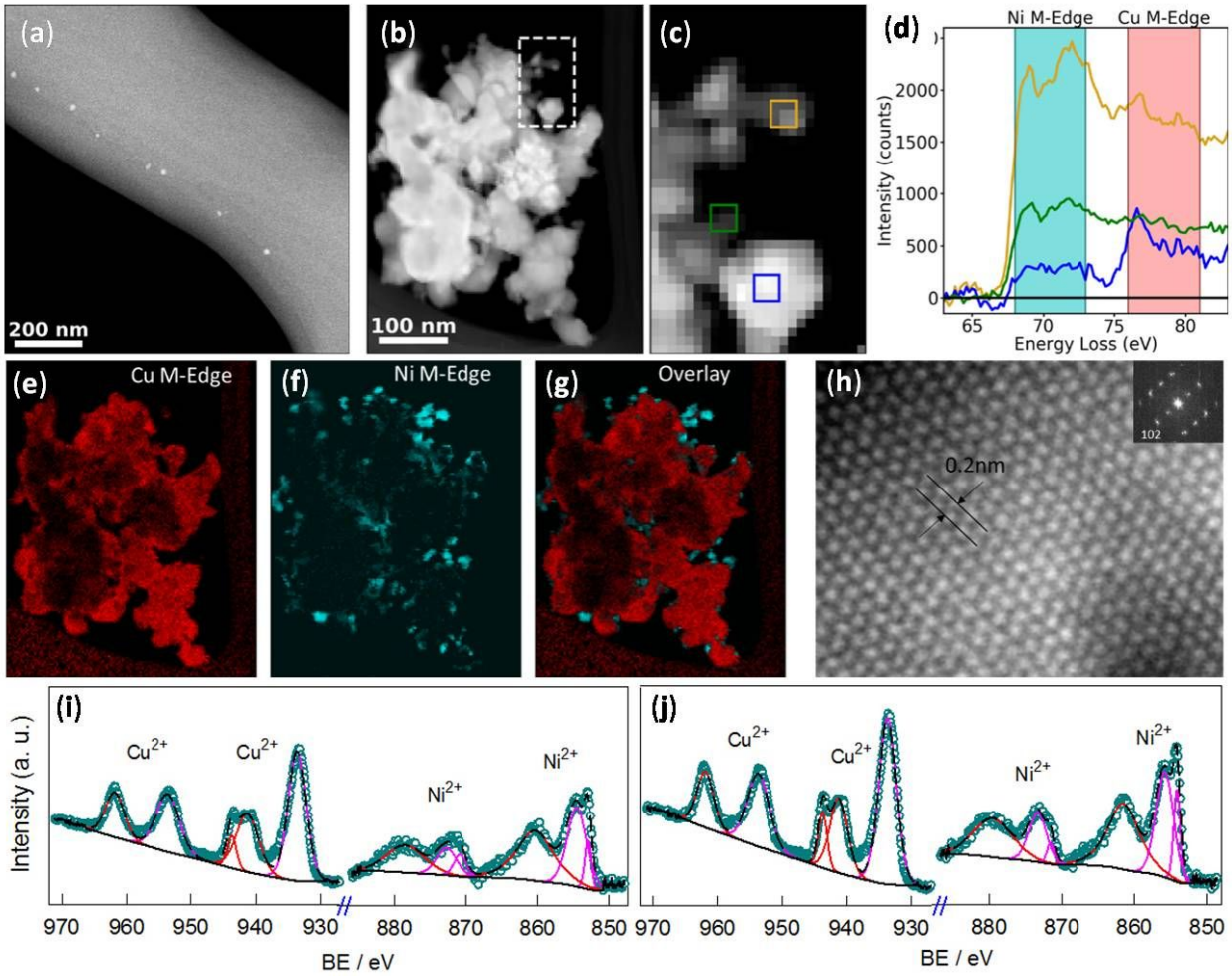

Figure 2. HR-TEM image of $Cu_{0.9}Ni_{0.1}O$ (a) along with STEM image (b, c), EELS signals (d), EDS elemental mapping for Cu M-edge (e), Ni M-edge (f), overlay (g) and high resolution planar image with its Fourier transform in the inset (h). Comparative high resolution XPS Cu(2p) and Ni(2p) spectra of $Cu_{0.95}Ni_{0.05}O$ (i) and $Cu_{0.9}Ni_{0.1}O$ (j) catalysts.

Further, core XPS spectra of Cu(2p) and Ni(2p) in $Cu_{0.95}Ni_{0.05}O$ and $Cu_{0.9}Ni_{0.1}O$ is shown in Figure 2(i,j). In both cases, the doublet of Cu(2p) showed two peaks with the binding energies at 933.3 and 953.4 eV are due to Cu ($2p_{3/2}$) and Cu ($2p_{1/2}$) of CuO, respectively.[41,42] Relatively higher binding energy peaks at 941.3 and 943.6 eV are shake up satellite peaks for Cu ($2p_{3/2}$) and

peak at 961.8 eV is the shakeup satellite peak for Cu ($2p_{1/2}$). Likewise, the binding energies of Ni(2p), after deconvolution, is found as the doublet of Ni ($2p_{3/2}$) at 852.9, 854.5 eV and of Ni ($2p_{1/2}$) at 870.8, 872.7 eV. Strong shake-up satellite peaks at 860.4 and 878.6 eV, respectively also appear as expected.[41,42] The broad peaks at 854.5 and 872.7 eV along with shoulder peaks at 852.9 and 870.8 eV are the unique features of NiO (related to Ni^{2+} state) and characteristic of bulk nickel oxide.[41,42] All these peaks collectively confirms the presence of free NiO on the surface. Further, both Cu and Ni are solely in +2 oxidation state in both the catalysts.

Electrochemical studies

Initially, continuous cyclic voltammetry (CV) behavior of undoped (CuO and NiO), Ni-substituted-CuO ($Cu_{0.95}Ni_{0.05}O$ and $Cu_{0.9}Ni_{0.1}O$) and Ni metal and NiO-deposited-CuO (Ni/CuO and NiO/CuO) drop-casted on glassy carbon electrode is studied in $NaHCO_3$ (0.5 M). Scan rate is kept at 40 mVs^{-1} for all the studies. This study is carried out to understand the basic electrochemical properties of the materials. In order to avoid the oxygen evolution and hydrogen evolution reactions, we restricted our working potential window from -0.8 V to 0.4 V vs. Ag/AgCl. In Figure 3(a), CV of CuO showed a diffused redox peak with enhanced anodic (i_{pa}) and cathodic (i_{pc}) current compared to glassy carbon electrode. Oxidation and reduction peak of Cu^{2+}/Cu^0 appears with the equilibrium potential ($E^{1/2}$) of 144 ± 2 mV with a peak-to-peak separation (ΔE_p) of 197 mV, measured from the last CV cycle. A characteristic pre-wave is also observed at -0.07 V due to the oxidation of Cu^0 to Cu^{1+} (Cu_2O).[32] The surface excess values (Γ), i.e., number of moles of active sites available on the electrode surface, is 0.45 nmol cm^{-2} (Figure S2(a)), using the equation: $\Gamma = Q/nFA$.[43] Here, Q is the charge obtained for the redox peak, n is the number of electrons involved, F is the faradaic constant and A is the area of the electrode. Likewise, the $Cu_{0.95}Ni_{0.05}O$ showed similar redox features with $E^{1/2}$ = 137 ± 2 mV and ΔE_p = 184

mV values (Figure 3b) and the calculated Γ value is 0.66 nmol cm^{-2} (Figure S2(b)). In comparison, CV of $Cu_{0.9}Ni_{0.1}O$ showed prominent redox peak at 0.051 and -0.192 volts. The enhancement in the anodic and cathodic current is due to Cu^{2+}/Cu^{0} redox reaction coupled with substituted Ni^{2+}/Ni^{0} (Figure 3c). Corresponding $E^{1/2}$ and ΔE_p values are 124 ± 2 mV and 147 mV with surface excess value (Γ) of 1.17 nmol cm^{-2} (Figure S2(c)). It is noteworthy that the current values of i_{pa} and i_{pc} and surface excess Γ value of $Cu_{0.9}Ni_{0.1}O$ is higher than $Cu_{0.95}Ni_{0.05}O$, with slight shifts (~13 ± 2 mV) in the peak potentials. This indicates more number of available active sites in the former due to higher Ni substitution. Comparatively, undoped CuO shows broad and less intense peaks with peak voltages shifted by ~20 mV. Since XRD has shown the presence of separated NiO phase (Figure 1b), CV of NiO alone and NiO deposited CuO (NiO/CuO) are studied in the similar potential range as control experiments. No redox feature is observed on NiO (Figure 3d), confirming that NiO phase is not a redox catalyst in the studied potential range. In case of NiO/CuO (Figure S2(d)), CV looks similar to CuO(Figure 3c) demonstrating no effect of NiO addition. CV for Ni metal supported CuO (Ni/CuO) is also performed as a control experiment (Figure S2(e)). This is carried out to rule out the presence of any undetected metallic nickel which may be present in the substituted compounds. In the CV, the redox features and the overall response is quite close to CuO with diminished peak intensity. These experiments clearly indicate the redox electrochemistry is only due to the interaction between substituted Ni^{2+} species and Cu^{2+} and not from the separated Ni/NiO or NiO/CuO phase.

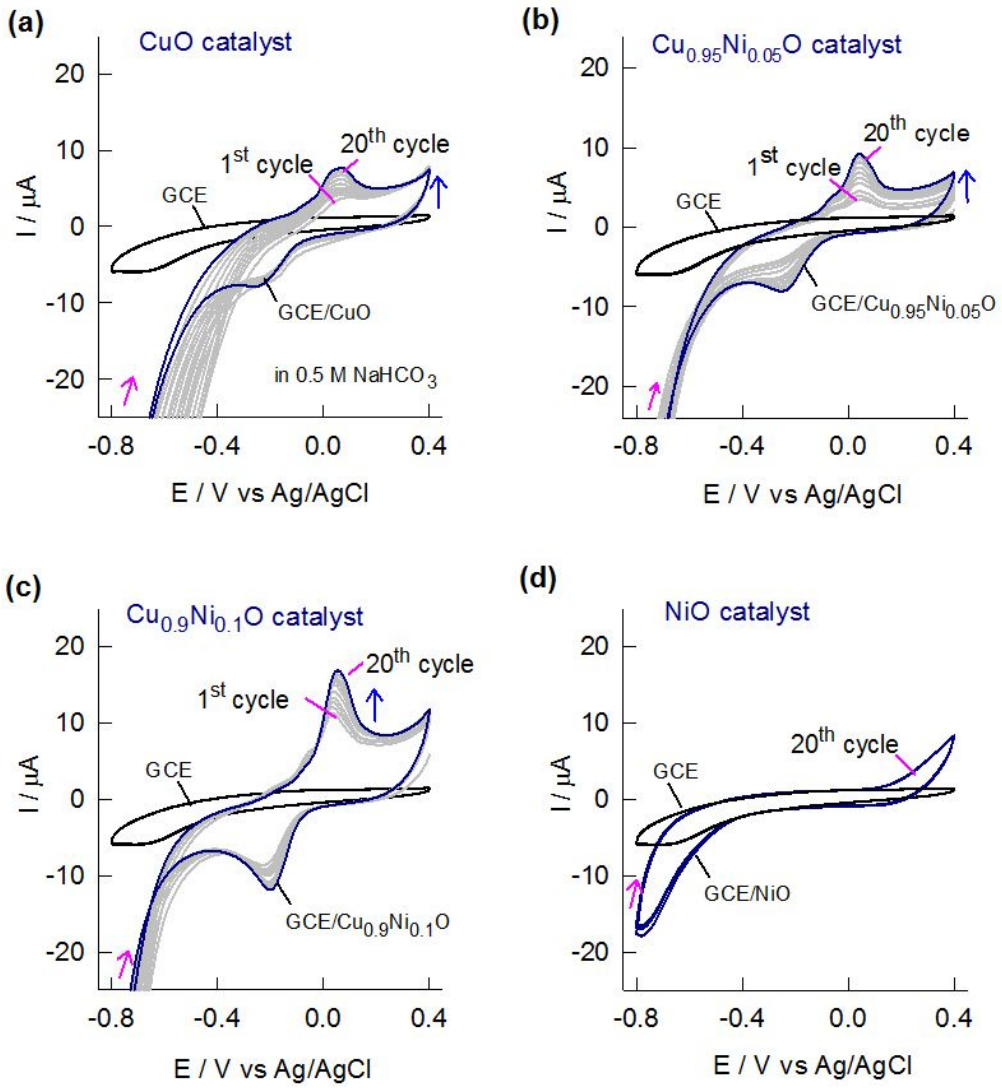

Figure 3. Continuous CV responses of CuO (a) $Cu_{0.95}Ni_{0.05}O$ (b), $Cu_{0.9}Ni_{0.1}O$ (c) and NiO (d) coated GCE along with bare GCE at a scan rate of 40 mV s^{-1} in 0.5 M $NaHCO_3$ electrolyte solution.

Further, the redox behavior and electron transfer properties of $Cu_{0.9}Ni_{0.1}O$ and $Cu_{0.95}Ni_{0.05}O$, and CuO is studied by varying the scan rates from 10 to 150 mVs^{-1} (Figure S3) and potential ranges between -0.8V≤ 0 ≤ 0.8V (Figure S4). While increasing scan rates (*ν*), the respective i_{pa} and i_{pc} currents at corresponding redox peaks, are increased significantly with slight shift in E_p and

changes in ΔE_p for all three electrocatalysts (Figure S3(a-c)). Presumably, the potential shifts may be due to the sluggish electron transfer kinetics due to semiconducting nature of the materials. A linear plot of peak current (i_p) versus square root of the scan rate ($v^{1/2}$) is drawn for $Cu_{0.9}Ni_{0.1}O$ (Figure S3(d)), $Cu_{0.95}Ni_{0.05}O$ (Figure S3(e)) and CuO (Figure S3(f)), respectively. The nature of this linearity is directly related to the sufficiently good conductivity of $Cu_{0.9}Ni_{0.1}O$ in the studied scan rates.

In addition, the influence of potential window on electrochemical behaviors, the CV of $Cu_{0.9}Ni_{0.1}O$, $Cu_{0.95}Ni_{0.05}O$ and CuO electrodes is recorded under various potential ranges (E= -0.8V≤ 0 ≤ 0.8V) at a scan rate of 40 mVs^{-1} (Figure S4). In the potential range of -0.4 to +0.4V, the CV of $Cu_{0.9}Ni_{0.1}O$ (Figure S4(a)) and $Cu_{0.95}Ni_{0.05}O$ (Figure S4(b)) show similar redox features as seen earlier. Once the potential window increased to -0.6 to +0.6V, the current values of i_{pa} and i_{pc} increased for both $Cu_{0.9}Ni_{0.1}O$ and $Cu_{0.95}Ni_{0.05}O$. Wider potential window allows the redox reaction to occur more profoundly causing the current to increase. This increase in current is more significant in for $Cu_{0.9}Ni_{0.1}O$. At more positive side (0 to +0.8V), bubbling can be seen in both electrodes due to oxygen evolution reaction (OER). In negative direction from 0 to -0.8V, featureless CV response with considerable reduction current at -0.8V is seen. Once the range is extended to -0.9V and -1V, a bubbling can be observed due to hydrogen evolution reaction (HER) in both the electrodes. Similar explanation holds true for CuO also however; the current densities are significantly lower that the Ni doped systems (Figure S4(c)). Following from the results, the potential range is fixed from -0.8 to +0.4V vs. Ag/AgCl, in order to avoid OER/HER electrochemical reactions.

Electrocatalytic CO_2 reduction

To examine the catalytic activity of all the prepared electrodes for CO_2 electroreduction, CV experiments were carried out in the N_2 (blank) and CO_2 saturated (purging for 30 mins) 0.5 M $NaHCO_3$ electrolyte at 20 mV s^{-1}. All the CVs are carried out in the potential range of 0.0 to -0.8 V vs. Ag/AgCl. Comparative CV responses of CuO (Figure 4a), $Cu_{0.95}Ni_{0.05}O$ (Figure 4b) $Cu_{0.9}Ni_{0.1}O$ (Figure 4c), and are shown in CO_2 and N_2 saturated solutions. Blank GCE response is also given with all the catalysts for comparison. In presence of CO_2, a broad cathodic response due to the electroreduction of CO_2 starts at an onset potential of about -0.54 V on CuO (Figure 4a). In $Cu_{0.95}Ni_{0.05}O$, the cathodic current in CO_2 saturated electrolytes is 0.18 mA which is about 9 times higher than the N_2 saturated electrolyte (Figure 4b). Similarly, in $Cu_{0.9}Ni_{0.1}O$, cathodic response with an onset voltage of -0.35 Vis attained (Figure 4c). Onset voltage is about 20 mV lower than undoped CuO demonstrating the catalytic effect of Ni^{2+} in CuO. Cathodic current at -0.8 V is 2.9 mA in CO_2 saturated solution. This is about 14 times higher than N_2 saturated solution confirming the high activity of $Cu_{0.9}Ni_{0.1}O$ for CO_2 electroreduction. Current density after normalizing the surface area gives about 20 times higher activity in the case of $Cu_{0.9}Ni_{0.1}O$ compared to CuO. Similar enhancement is about 15 times in the case of $Cu_{0.95}Ni_{0.05}O$ compared to CuO. Interestingly, pure NiO is non-catalytic towards CO_2 electroreduction and show almost no change in current in CO_2 saturated electrolyte compared to N_2 saturated electrolyte (Figure S5(a)). In order to ascertain that the catalysis is truly due to the substituted Ni^{2+} and Cu^{2+} interaction, CV experiment with NiO supported CuO (NiO/CuO) and Ni metal supported CuO (Ni/CuO) are also carried out (Figure S5(b) and (c)). The CO_2 electroreduction current with NiO/CuO is 0.125 mA at -0.8 V. It is 0.06 mA with Ni/CuO catalyst. Current values over supported catalysts are much lower than the Ni substituted catalysts ($Cu_{0.95}Ni_{0.05}O$ and $Cu_{0.9}Ni_{0.1}O$). These observations indicate that synergetic ionic interaction between Cu^{2+} and Ni^{2+}

is indeed is the major contributor for the observed enhanced activity. NiO/CuO and Ni/CuO are on the other hand, minor contributor. Further, the estimated BET surface area of $Cu_{0.95}Ni_{0.05}O$ and $Cu_{0.9}Ni_{0.1}O$ are about 5 times lower than CuO, therefore, the high activity of the doped compounds is truly due to ionically substituted Ni in CuO. All the current values as a result of CO_2 electroreduction are normalized and compared with respect to BET surface areas (Table S2). Cleary, doped compounds are remarkably higher active than CuO, Ni/CuO and NiO/CuO further highlighting the importance of the ionic interaction for superior activity.

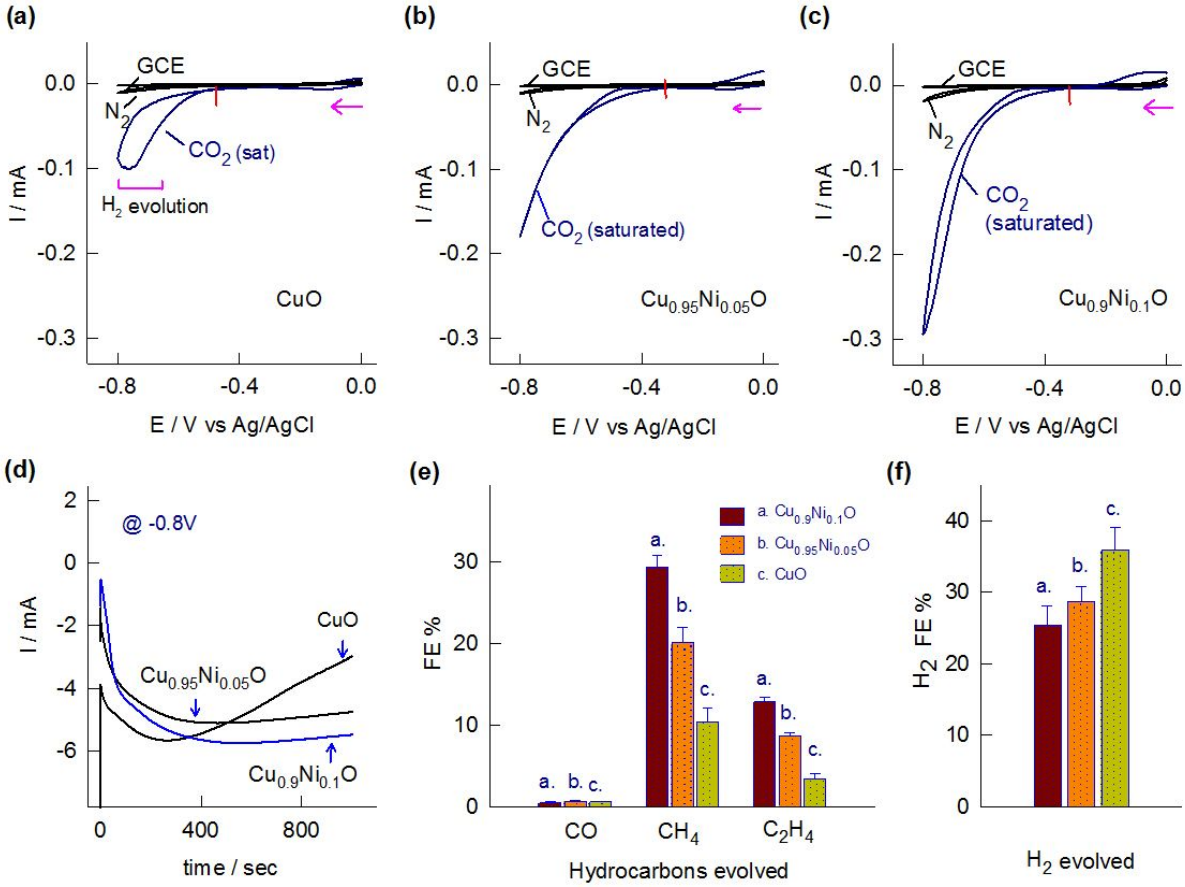

Figure 4. Electroreduction CV response of CuO (a), $Cu_{0.95}Ni_{0.05}O$ (b) and $Cu_{0.9}Ni_{0.1}O$ (c) in CO_2 saturated (for 30 mins) 0.5 M $NaHCO_3$ electrolyte solutionsat a scan rate 20 mVs^{-1}. Chronoamperometric responses of CuO, $Cu_{0.95}Ni_{0.05}O$ and $Cu_{0.9}Ni_{0.1}O$, at a fixed potential of -

0.8 V vs. Ag/AgCl (i.e., -0.2 V RHE) for 1000 seconds (d) in CO_2 saturated 0.5 M $NaHCO_3$ electrolyte solution. Bar diagram (with errors) for the faradaic efficiencies of their respective carbonaceous species (e) and hydrogen (f) gaseous products detected in gas chromatography.

Steady state current responses for all the three catalysts in CO_2 saturated electrolyte at -0.8V vs. Ag/AgCl (-0.2 V RHE), is shown in Figure 4(d). Initially the current decreased gradually up to 400 s and attained steady state with a current value of 5.6 mA and 4.8 mA for $Cu_{0.9}Ni_{0.1}O$ and $Cu_{0.95}Ni_{0.05}O$, respectively. This indicates that both the catalysts are stable and $Cu_{0.9}Ni_{0.1}O$ has higher electroreduction activity for CO_2. In contrast, the CuO initially showed a characteristic decrease followed by increase in current depicting an oxidation behavior. Steady state is not attained even after 1000 seconds due to the instability of the CuO. In addition, CV is carried out after this chronoamperometric experiment for $Cu_{0.9}Ni_{0.1}O$ and CuO (Figure S6). It is observed that the redox behavior of $Cu_{0.9}Ni_{0.1}O$ is preserved whereas it is diminished in CuO. This highlights the Ni^{2+} substitution in CuO on one-hand increases the activity and on the other-hand imparts the stability.

In order to analyze the products formed after CO_2 reduction, the evolved gases were collected by an air-lock syringe and the products were subjected to gas chromatography. The major gaseous products on all there electrocatalysts are CO, CH_4, C_2H_4 and H_2. The liquid sample was also collected and subjected to GC equipped with liquid detection capability. Exclusively, ethanol was detected. Since most of the copper based electrocatalysts have been pronounced for the formation of CH_4 and C_2H_4 with H_2 as the side product, it is interesting to note that Ni substitution in CuO suppresses the hydrogen production significantly. This is also depicted in terms of percent Faradaic efficiencies (FE %) for majorly gaseous products as shown in Figure 4(e,f). FE % of CO is same (1.0 %), for all the three catalysts as the copper based catalysts do not favor CO formation.[32] Comparatively, the formation of CH_4 and C_2H_4 predominantly occurs on

$Cu_{0.9}Ni_{0.1}O$ with FE % up to 29.4 % and 12.8 %, respectively (Figure 4e).The same was 20.2 % and 8.7 % for $Cu_{0.95}Ni_{0.05}O$. On CuO, the FE% for CH_4 and C_2H_4 is 3 and 4 times lower than $Cu_{0.9}Ni_{0.1}O$. Inferior hydrocarbon FE % with CuO is due to the undesired HER and possibly a different mechanism. The FE % for ethanol was 15.3% on $Cu_{0.9}Ni_{0.1}O$ giving the total faradaic efficiency 83.7%. FE % for hydrogen on $Cu_{0.95}Ni_{0.05}O$ and $Cu_{0.9}Ni_{0.1}O$ is 25.4 % and 28.7 %, much lower than CuO (35.9 %) as in Figure 4f. Thus, the presence of Ni in CuO host enhances the formation of hydrocarbons while suppressing the hydrogen production.

Comparative electrocatalytic performance of the $Cu_{0.9}Ni_{0.1}O$ catalyst with literature is available in Table S3 (supporting information). From the table it is also clear that hydrocarbon efficiency of the doped catalyst is comparable or better at much lower applied potential. Total FE % is 58 to 68 % for both the Ni substituted catalysts as only the gaseous products are analyzed. Very importantly, both $Cu_{0.95}Ni_{0.05}O$ and $Cu_{0.9}Ni_{0.1}O$ are able to generate hydrocarbons at -0.2 V (RHE) which is so far the lowest. In terms of overpotential, this is about 370 mV for methane and 280 mV for ethylene. To the best of our knowledge, this is the lowest overpotential ever reported. From Table S3, the lowest potential is -1.1 V (RHE) for methane and ethylene production. This is higher by 0.9 V than $Cu_{0.95}Ni_{0.05}O$ and $Cu_{0.9}Ni_{0.1}O$, a very significant gain in voltage. The materials used in this study are highly crystalline bulk materials. Clearly, apart from ionic interaction, crystallinity is possibly another important factor which reduces the overvoltage for this reaction.

The stability of $Cu_{0.9}Ni_{0.1}O$ catalyst is studied by depositing it onto FTO electrode and subjected to post-XRD and XPS after chronoamperometry in CO_2 saturated solution for 1000 sec (Figure S7 & S8). It is observed that apart from FTO peaks, $Cu_{0.9}Ni_{0.1}O$ peaks are retained before and after CO_2 electrocatalysis confirming the stability of the bulk structure of $Cu_{0.9}Ni_{0.1}O$ catalyst

(Figure S7). The XPS also confirms the stability of the $Cu_{0.9}Ni_{0.1}O$ catalyst surface as shown in Figure S8. XPS of as prepared catalysts is also given for comparison. It is worth noticing that there is no change in the XPS spectra before and after the chronoamperometry. Both copper and nickel show same oxidations state before and after the experiments proving the stability of $Cu_{0.9}Ni_{0.1}O$ catalysts.

In order to access the stability under a more rigorous reductive treatment, CuO and $Cu_{0.9}Ni_{0.1}O$ were subjected to chronoamperometry at -0.8 V for 2 hours. The CV after this treatment is shown in Figure S9. The behavior in both the material confirms the formation of metallic copper[44]. This behavior confirms that the catalysts are unstable under long reductive treatment.

It is speculated that improvement in hydrocarbon selectivity along with the HER suppression is due to modification in the mechanism which is investigated by *in situ* FTIR and DFT studies. Mechanistic investigation for the CO_2 electroreduction pathways over CuO and $Cu_{0.9}Ni_{0.1}O$ is executed using DRIFT *in situ* FTIR experiment (Figure 5). The schematic representation of DRIFT cell is displayed in Figure 5a. As the copper based materials are known for converting CO_2 to hydrocarbons both thermally and electrochemically, it is assumed that thermal reduction of CO_2 with gaseous hydrogen is similar to electrochemical reduction of CO_2. Firstly, the interaction of H_2 over CuO and $Cu_{0.9}Ni_{0.1}O$ is investigated in the range of 2400 to 3200 cm^{-1} (Figure 5b). IR spectra of both as prepared sample show no indication of any band in the flow of nitrogen at room temperature. On passing H_2, the DRIFT spectra of $Cu_{0.9}Ni_{0.1}O$, showed weak bands in the range of 2800 -3000 cm^{-1} at 50°C. This band is due to the formation of formate on the surface by utilizing the atmospheric CO_2.[45] The similar band on CuO is considerably higher than $Cu_{0.9}Ni_{0.1}O$ under the same conditions. Same band at 100°C show

increase in the intensity on both the catalyst but intensity is still higher on CuO. At 200°C, intensity of formate diminishes significantly over $Cu_{0.9}Ni_{0.1}O$ but not much change is observed in the case of CuO. Temperature higher than 300°C causes complete disappearance of formate band on both the catalysts (Figure S10). To be precise, formate band disappears at 400°C on $Cu_{0.9}Ni_{0.1}O$ and at 500°C on CuO.

These experimental observations suggest that formate bands are more stable and prominent on CuO surface than $Cu_{0.9}Ni_{0.1}O$. Once Ni is substituted in CuO matrix, formate band are less stable and less prominent. Similar observation can also be drawn when the mixture of H_2 and CO_2 (1:1) is reacted on the catalyst's surface (Figure 5c). In this case also, over all intensity of formate band is less prominent on $Cu_{0.9}Ni_{0.1}O$ compared to CuO. Intensity differences in the formate can be prominently observed at 100, 200 and 300°C.

In the light of above observations, one can confirm that Ni substitution in CuO affects the catalyst's ability to stabilize formate (Figure 5d). This demonstrates the mechanistic differences between the two catalysts in which CuO shows the dominant formate pathway compared to $Cu_{0.9}Ni_{0.1}O$. Dominance of formate pathway with the generation of H_2 can be correlated well in the light of quantum mechanical calculations carried out by Cheng et. al.[46] This study reveals two pathways in copper based materials; one is dominatingly forming formate and other forming CO. The pathway leading to CO eventually leads to hydrocarbon formation while more formate leads to more hydrogen. This correlates well with the FTIR studies establishing that that Ni substitution in CuO shows less contribution from formate pathway resulting in less hydrogen formation and due to this more hydrocarbons. CuO on the other hand shows more contribution from formate pathway resulting into fewer hydrocarbons and more hydrogen generation.

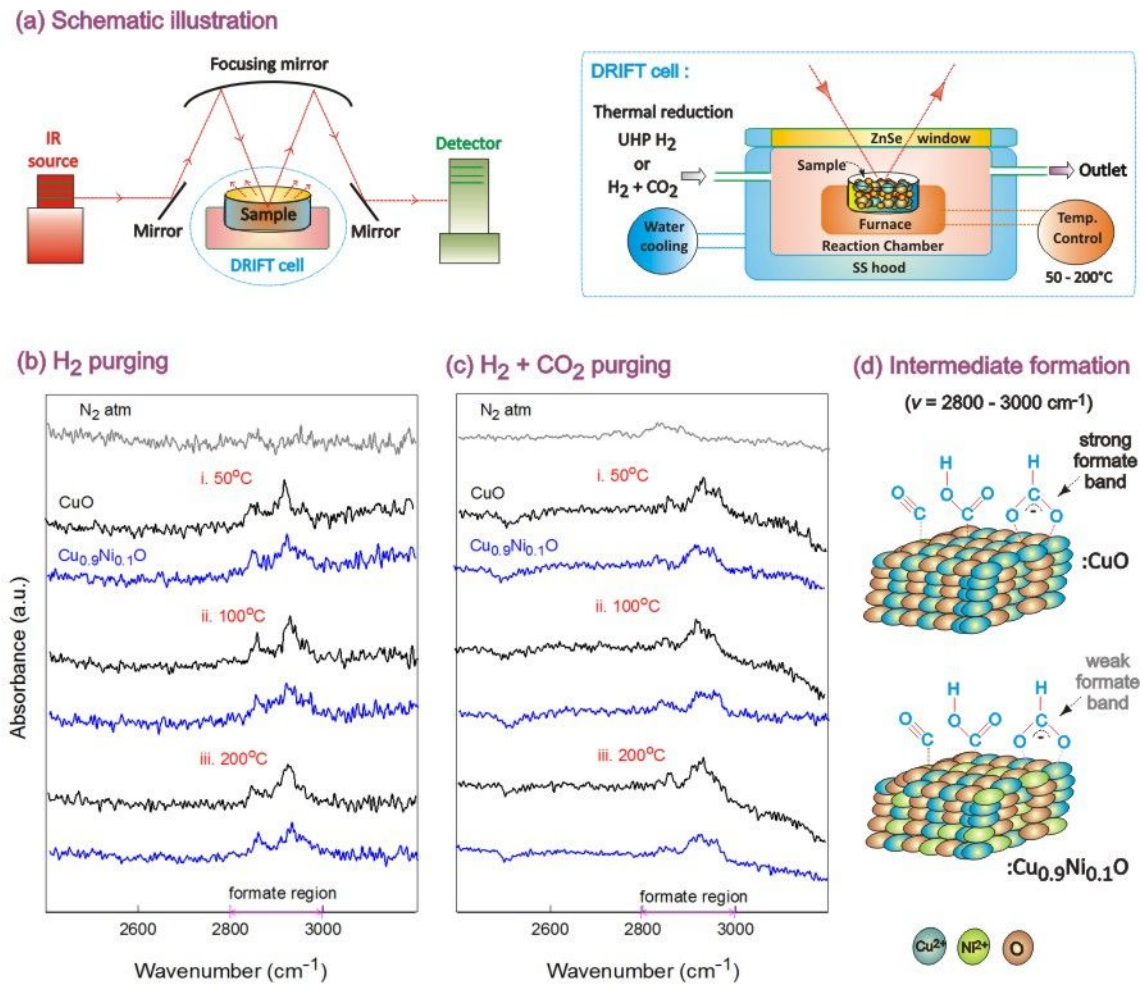

Figure 5. Schematic representation of DRIFT-FTIR spectroscopy (a), DRIFT spectra recorded in IR ranges (2400 to 3200 cm^{-1}) on passing H_2 (b) and CO_2+H_2 UHP gases (c) over KBr mixed $Cu_{0.9}Ni_{0.1}O$ and CuO catalysts at different temperatures from 50 to 200°C. Possible intermediates formed on pure copper oxide (CuO) and Nickel doped copper oxide catalysts (d).

Further, Density functional theory (DFT) was used for theoretical calculations (Figure 6), implemented in the CO_2 electroreduction pathways on CuO and $Cu_{0.9}Ni_{0.1}O$ model catalysts (Figure S11-13). The optimized lattice parameters of bulk monoclinic CuO (space group – *C2/c*) were found to be: a = 4.37, b = 3.86, and c = 3.92 Å (Figure S11,12), in excellent agreement with previous reports.[47-48] The (111) facet of CuO was chosen for calculations, as it has been found to be the most stable facet of CuO with lowest surface energy.[47] It contained 128 (64 Cu and 64 O)

atoms. The Ni-doped structure contained 60 Cu and 4 Ni atoms, so the stoichiometry of alloy turned out to be $Cu_{0.9375}Ni_{0.0625}O$ (Figure S13). Only one composition of Ni-doping was taken, as it is enough to observe the qualitative effect of change in the catalytic activity upon alloying.

The carbon dioxide electro-reduction to methane formation involves 7 intermediates (8-electron transfer process)[49]. The (111) surface of CuO contains 4 types of active sites – coordinatively saturated Cu (Cu_{CSA}), coordinatively unsaturated Cu (Cu_{CUS}), surface O (O_{SUB}), and subsurface O (O_{SUF})[47] (Figure S11(a)). The *COOH, *CO and *CHO intermediates which adsorb through C were relaxed on O_{SUF} sites, while those that bind through O (i.e., $*CH_2O$, $*CH_3O$, *O, and *OH) were relaxed on Cu_{CUS} sites (Figure S14), since Cu_{CUS} and O_{SUF} are more active than their corresponding saturated sites.[47] For the case of (111) surface of $Cu_{0.9375}Ni_{0.0625}O$, we only relaxed these intermediates in the vicinity of Ni atom as shown in Figure S15 to determine the effect of Ni doping. The intermediate adsorption energies (E_{ads}^{DFT}) were calculated for these completely relaxed structures using the equations (S1-S7). From these intermediate adsorption energies, Gibb's free energies of adsorption (G^*) were calculated according to the expression[50-51]:

$$G^* = E_{ads}^{DFT} + \Delta ZPE - T\Delta S - eU \qquad (2)$$

where ΔZPE, ΔS, e, and $U$are the difference in zero-point energies and vibrational entropies between reactants and products, number of electrons transferred, and applied potential. The value of temperature (T) has been taken to be 300 K. The values of E_{ads}^{DFT}, ZPE, and TS for reference molecules and intermediates are tabulated in Tables S4-S6.

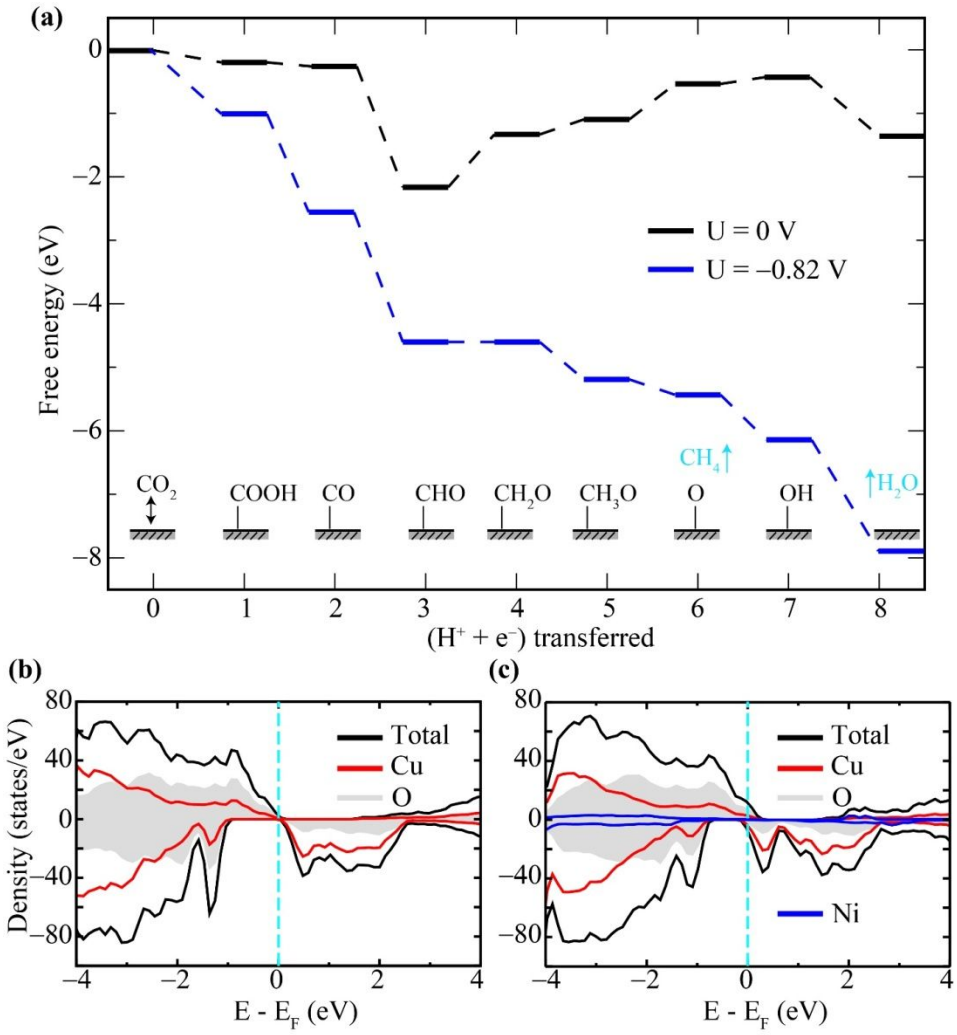

Figure 6. Free energy diagram for CO_2 electroreduction to CH_4 on (111) surface of $Cu_{0.9375}Ni_{0.0625}O$(a). PDOS of (111) surfaces of CuO (b) and $Cu_{0.9375}Ni_{0.0625}O$ (c).

The free energy diagrams for electroreduction of CO_2 to CH_4 on CuO and $Cu_{0.9375}Ni_{0.0625}O$ catalyst surfaces are plotted in Figures 6(a) and S16, respectively, following the approach taken in previous reports.[50-51] The potential determining step (PDS) for this reaction is conversion of *CHO to *CH_2O on both pristine and doped catalyst surfaces, with $Cu_{0.9375}Ni_{0.0625}O$ exhibiting lower barrier for this step (0.82 eV) than the CuO catalyst (1.15 eV). Therefore, limiting potential (U_L), which is numerically equal to negative of the barrier of PDS[50], values for CuO and $Cu_{0.9375}Ni_{0.0625}O$ catalysts come out to be -1.15 and -0.82 V, respectively. If the value of U_L

is higher, the overall reaction becomes exergonic (i.e., downhill in free energy) at a lower external potential. Hence, the efficiency of CO_2 electroreduction to methane will be higher for $Cu_{0.9375}Ni_{0.0625}O$ as compared to the pristine CuO catalyst, in agreement with the experiments. The lower barrier for PDS observed in the case of $Cu_{0.9375}Ni_{0.0625}O$ can be explained from adsorption energies of *CHO and *CH_2O intermediates on the two catalysts as shown in Tables S5 and S6. The *CHO intermediate is more destabilized on the surface of $Cu_{0.9375}Ni_{0.0625}O$, while there is stabilization for the case of *CH_2O intermediate on its surface. The increased catalytic activity on the Ni-doped CuO can also be rationalized on the basis of change in electronic properties of CuO upon alloying. For this purpose, the partial density of states (PDOS) has been plotted for both surfaces in Figure 6(b,c). Pristine CuO surface is a small band gap semiconductor with the valence band states mostly contributed by O, and the conduction band states mostly contributed by Cu. The system becomes conducting upon doping with Ni, therefore finite states present at the Fermi level is responsible for the increased activity of Ni-doped CuO system, due to better interaction with the adsorbates.[52]

CONCLUSION

In summary, we have synthesized Ni-substituted-CuO ($Cu_{1-x}Ni_xO$; x= 0.05 and 0.1) and CuO catalysts by solution combustion method. Collective characterizations such as XRD, FESEM-EDS, HRTEM-STEM, EELS, EDS and XPS conclude the bulk substitution of Ni^{2+} in CuO host. Electrochemical studies of $Cu_{0.9}Ni_{0.1}O$, $Cu_{0.95}Ni_{0.05}O$ show remarkable redox active behavior and superior electrocatalytic activity compared to CuO signifying the importance of substitution of ionic nickel. It is worth noticing that $Cu_{0.9}Ni_{0.1}O$ and $Cu_{0.95}Ni_{0.05}O$ electrocatalytic activity than Ni metal and NiO supported CuO. This proves that ionic interaction between Ni^{2+} and Cu^{2+} is vital for the high activity. Ni or NiO supported CuO lacks this interaction therefore do not

display high activity. Steady state chronoamperometry at a fixed potential of -0.8$V_{Ag/AgCl}$ (i.e., -0.2 V_{RHE}) in CO_2 saturated electrolyte also revels high activity and stability of nickel doped catalysts ($Cu_{0.9}Ni_{0.1}O$, $Cu_{0.95}Ni_{0.05}O$). Remarkable improvement is noticed in the selectivity or faradaic efficiency of hydrocarbons. The FE % of H_2 on$Cu_{0.9}Ni_{0.1}O$, $Cu_{0.95}Ni_{0.05}O$ was suppressed effectively compared to CuO. The observed hydrocarbon efficiency is achieved at lowest possible over voltage. A voltage gain of about 0.9 V is achieved compared to the best reported catalysts. Simultaneously, the hydrocarbon selectivity is markedly improved. The FE % of CH_4 and C_2H_4 is 29.4 % and 12.8 % on $Cu_{0.9}Ni_{0.1}O$ which is about 3 and 4 times higher than CuO. These improvements are attributed to the mechanistic difference between substituted and unsubstituted catalysts. Mechanistic studies by the *in situ* DRIFT infer that $Cu_{0.9}Ni_{0.1}O$ has fewer propensities towards formate intermediate compared to CuO. This leads to high hydrocarbon selectivity and lesser hydrogen formation. The free energy diagrams computed using DFT confirms that the Ni-doped CuO electrocatalyst is thermodynamically more active than pristine CuO, owing to its lower theoretical overpotential.

ASSOCIATED CONTENT

The Supporting Information is available free of charge on the ACS Publications websites. Experimental characterization like Reitveld refinements, CV responses of $Cu_{0.90}Ni_{0.10}O$, $Cu_{0.95}Ni_{0.05}O$, CuO (surface excess values), and Ni/NiO-deposited CuO, effect of scan rate and potential window, electrocatalytic reduction of CO_2 responses on NiO, Ni/NiO-deposited-CuO catalysts, post XRD,XPS and CV data, DRIFT-FTIR spectra, normalized current density, DFT calculation details with tabulations and comparative table for the electrocatalytic performance of $Cu_{0.90}Ni_{0.10}O$ catalyst (PDF).

AUTHOR INFORMATION

*Corresponding Author

E-mail: ssharma@iitgn.ac.in (S.S), chandra.tiwary@metal.iitkgp.ac.in (C.S.T), abhishek@iisc.ac.in (A.K.S)

AUTHOR CONTRIBUTIONS

S.S. and S.N. envisaged the idea and executed the experiments. R.K., A.K.S. and C.S.T. carried out DFT calculations. C.S. performed Reitveld refinement studies. S.I. performed XPS analysis. J.A.H. and J.C.I. performed the transmission microscopy experiments. All the authors contributed to the data analysis and writing and gave approval for the final submission.

CONFLICT OF INTEREST

The authors declare no conflict of interest.

ACKNOWLEDGEMENTS

S.S. and S.N. gratefully acknowledges IIT Gandhinagar and DST-SERB sponsored research project (EMR/2016/000806) for funding and fellowship. A portion of the microscopy was performed as part of a user proposal at Oak Ridge National Laboratory's Center for Nanophase Materials Sciences (CNMS), which is a U.S. Department of Energy, Office of Science User Facility. R.K and A.K.S acknowledge computational facilities provided by Materials Research Centre, Solid State and Structural Chemistry Unit, and Supercomputer Education and Research Centre at Indian Institute of Science.

REFERENCES

(1) Kumar, B.; Brian, J. P.; Atla, V.; Kumari, S.; Bertram, K. A.; White, R. T.; Spurgeon, J. M. New Trends in the Development of Heterogeneous Catalysts for Electrochemical CO_2 Reduction. *Catal. Today* **2016,** *270*, 19-30.

(2) Zhu, D. D.; Liu, J. L.; Qiao, S. Z. Recent Advances in Inorganic Heterogeneous Electrocatalysts for Reduction of Carbon Dioxide. *Adv. Mater.* **2016,** *28* (18), 3423-3452.

(3) Porosoff., M. D.; Yan., B.; Chen., J. G. Catalytic Reduction of CO_2 by H_2 for Synthesis of CO, Methanol and Hydrocarbons: Challenges and Opportunities. *Energy Environ. Sci.* **2016,** *9*, 62-73.

(4) Boston., D. J.; Xu., C.; Armstrong., D. W.; MacDonnell., F. M. Photochemical Reduction of Carbon Dioxide to Methanol and Formate in a Homogeneous System with Pyridinium Catalysts. *J. Am. Chem. Soc.* **2013,** *135*, 16252−16255.

(5) Richardson., R. D.; Holland., E. J.; Carpenter., B. K. A Renewable Amine for Photochemical Reduction of CO_2. *Nature Chem.* **2011,** *3*, 301-303.

(6) Yang, N.; Waldvogel, S. R.; Jiang, X. Electrochemistry of Carbon Dioxide on Carbon Electrodes. *ACS Appl. Mater. Interfaces* **2016,** *8* (42), 28357-28371.

(7) Qiao, J.; Liu, Y.; Hong, F.; Zhang, J. A Review of Catalysts for the Electroreduction of Carbon Dioxide to Produce Low-carbon Fuels. *Chem. Soc.Rev.* **2014,** *43* (2), 631-675.

(8) Britovsek., G. J. P.; Bruce., M.; Gibson., V. C.; Kimberley., B. S.; Maddox., P. J.; Mastroianni., S.; McTavish., S. J.; Redshaw., C.; Solan., G. A.; Strömberg., S.; White., A. J. P.; Williams, D. J. Iron and Cobalt Ethylene Polymerization Catalysts Bearing 2,6-Bis(Imino)Pyridyl Ligands: Synthesis, Structures, and Polymerization Studies. *J. Am. Chem. Soc.* **1999,** *121*, 8728-8740.

(9) Wang, Z.-L.; Li, C.; Yamauchi, Y. Nanostructured Nonprecious Metal Catalysts for Electrochemical Reduction of Carbon Ddioxide. *Nano Today* **2016,** *11* (3), 373-391.

(10) Hossain, M. N.; Wen, J.; Konda, S. K.; Govindhan, M.; Chen, A. Electrochemical and FTIR Spectroscopic Study of CO_2Reduction at a Nanostructured Cu/Reduced Graphene Oxide Thin Film. *Electrochem. Communi.***2017,** *82*, 16-20.

(11) Chen, C. S.; Handoko, A. D.; Wan, J. H.; Ma, L.; Ren, D.; Yeo, B. S. Stable and Selective Electrochemical Reduction of Carbon Dioxide to Ethylene on Copper Mesocrystals. *Catal. Sci. Techno.***2015,** *5* (1), 161-168.

(12) Kuhl, K. P.; Cave, E. R.; Abram, D. N.; Jaramillo, T. F. New Insights into the Electrochemical Reduction of Carbon Dioxide on Metallic Copper Surfaces. *Energy Environ. Sci.* **2012,** *5* (5), 7050-7059.

(13) Hori., Y.; Takahashi., R.; Yoshinami., Y.; Murata, A. Electrochemical Reduction of CO_2 at a Copper Electrode. *J. Phys. Chem. B* **1997,** *101*, 7075-7081.

(14) Kudo., A.; Nakagawa., S.; Tsuneta., A.; Sakata, T. Electrochemical Reduction of High Pressure CO_2on Ni Electrodes. *J. Electrochem. Soc.* **1993,** *140* (6), 1541-1545.

(15) Zhu, W.; Zhang, Y. J.; Zhang, H.; Lv, H.; Li, Q.; Michalsky, R.; Peterson, A. A.; Sun, S. Active and Selective Conversion of CO_2 to CO on Ultrathin Au Nanowires. *J. Am. Chem. Soc.* **2014,** *136* (46), 16132-16135.

(16) Kim, C.; Eom, T.; Jee, M. S.; Jung, H.; Kim, H.; Min, B. K.; Hwang, Y. J. Insight into Electrochemical CO_2 Reduction on Surface-Molecule-Mediated Ag Nanoparticles. *ACS Catal.* **2017,** *7* (1), 779-785.

(17) Zhang, S.; Kang, P.; Meyer, T. J. Nanostructured Tin Catalysts For Selective Electrochemical Reduction of Carbon Dioxide To Formate. *J. Am. Chem. Soc.* **2014,** *136* (5), 1734-1737.

(18) Detweiler, Z. M.; White, J. L.; Bernasek, S. L.; Bocarsly, A. B. Anodized Indium Metal Electrodes For Enhanced Carbon Dioxide Reduction In Aqueous Electrolyte. *Langmuir* **2014,** *30* (25), 7593-7600.

(19) Gao, D.; Zhou, H.; Wang, J.; Miao, S.; Yang, F.; Wang, G.; Bao, X. Size-dependent Electrocatalytic Reduction of CO_2 Over Pd Nanoparticles. *J. Am. Chem. Soc.* **2015,** *137* (13), 4288-4291.

(20) Kim, D.; Resasco, J.; Yu, Y.; Asiri, A. M.; Yang, P. Synergistic Geometric And Electronic Effects For Electrochemical Reduction Of Carbon Dioxide Using Gold-Copper Bimetallic Nanoparticles. *Nature Communi.***2014,** *5*, 4948-4956.

(21) Rasul, S.; Anjum, D. H.; Jedidi, A.; Minenkov, Y.; Cavallo, L.; Takanabe, K. A Highly Selective Copper-Indium Bimetallic Electrocatalyst For The Electrochemical Reduction Of Aqueous CO_2 to CO. *Angew. Chem. Int. Ed. Engl.* **2015,** *54* (7), 2146-2150.

(22) Ren, D.; Ang, B. S.-H.; Yeo, B. S. Tuning the Selectivity of Carbon Dioxide Electroreduction toward Ethanol on Oxide-Derived Cu_xZn Catalysts. *ACS Catal.* **2016,** *6* (12), 8239-8247.

(23) Clark, E. L.; Hahn, C.; Jaramillo, T. F.; Bell, A. T. Electrochemical CO_2 Reduction over Compressively Strained CuAg Surface Alloys with Enhanced Multi-Carbon Oxygenate Selectivity. *J. Am. Chem. Soc.* **2017,** *139* (44), 15848-15857.

(24) Chen, D.; Yao, Q.; Cui, P.; Liu, H.; Xie, J.; Yang, J. Tailoring the Selectivity of Bimetallic Copper–Palladium Nanoalloys for Electrocatalytic Reduction of CO_2 to CO. *ACS Appl. Energy Mater.* **2018,** *1* (2), 883-890.

(25) Mandal, L.; Yang, K. R.; Motapothula, M. R.; Ren, D.; Lobaccaro, P.; Patra, A.; Sherburne, M.; Batista, V. S.; Yeo, B. S.; Ager, J. W.; Martin, J.; Venkatesan, T. Investigating the Role of Copper Oxide in Electrochemical CO_2 Reduction in Real Time. *ACS Appl. Mater. Interfaces* **2018,** *10* (10), 8574-8584.

(26) Ren, D.; Deng, Y.; Handoko, A. D.; Chen, C. S.; Malkhandi, S.; Yeo, B. S. Selective Electrochemical Reduction of Carbon Dioxide to Ethylene and Ethanol on Copper(I) Oxide Catalysts. *ACS Catal.***2015,** *5* (5), 2814-2821.

(27) Chi., D.; Yang., H.; Du., Y.; Lv., T.; Sui., G.; Wang., H.; Lu., J. Morphology-controlled CuO Nanoparticles for Electroreduction of CO_2 to Ethanol *RSC Adv.* **2014,** *4*, 37329-37332.

(28) Yano, J.; Morita, T.; Shimano, K.; Nagami, Y.; Yamasaki, S. Selective Ethylene Formation By Pulse-Mode Electrochemical Reduction Of Carbon Dioxide Using Copper And Copper-Oxide Electrodes. *J. Solid State Electrochem.***2006,** *11* (4), 554-557.

(29) Eilert, A.; Cavalca, F.; Roberts, F. S.; Osterwalder, J.; Liu, C.; Favaro, M.; Crumlin, E. J.; Ogasawara, H.; Friebel, D.; Pettersson, L. G.; Nilsson, A. Subsurface Oxygen in Oxide-Derived Copper Electrocatalysts for Carbon Dioxide Reduction. *J. Phys. Chem. Lett.* **2017,** *8* (1), 285-290.

(30) Handoko, A. D.; Chan, K. W.; Yeo, B. S. –CH3 Mediated Pathway for the Electroreduction of CO_2 to Ethane and Ethanol on Thick Oxide-Derived Copper Catalysts at Low Overpotentials. *ACS Energy Lett.***2017,** *2* (9), 2103-2109.

(31) Li, C. W.; Kanan, M. W. CO_2Reduction At Low Overpotential on Cu Electrodes Resulting from the Reduction of Thick Cu_2O Films. *J. Am. Chem. Soc.* **2012,** *134* (17), 7231-7234.

(32) Li, Q.; Fu, J.; Zhu, W.; Chen, Z.; Shen, B.; Wu, L.; Xi, Z.; Wang, T.; Lu, G.; Zhu, J. J.; Sun, S. Tuning Sn-Catalysis for Electrochemical Reduction of CO_2 to CO via the Core/Shell Cu/SnO_2 Structure. *J. Am. Chem. Soc.* **2017,** *139* (12), 4290-4293.

(33) Huo, S.; Weng, Z.; Wu, Z.; Zhong, Y.; Wu, Y.; Fang, J.; Wang, H. Coupled Metal/Oxide Catalysts with Tunable Product Selectivity for Electrocatalytic CO_2 Reduction. *ACS Appl. Mater.Interfaces* **2017,** *9* (34), 28519-28526.

(34) Zhao, Y.; Wang., C.; Wallace., G. G. Tin Nanoparticles Decorated Copper Oxide Nanowires for Selective Electrochemical Reductionof Aqueous CO_2 to CO. *J. Mater. Chem. A* **2016,** *4*, 10710-10718.

(35) Upham, D. C.; Derk, A. R.; Sharma, S.; Metiu, H.; McFarland, E. W. CO_2Methanation by Ru-doped Ceria: The Role of the Oxidation State of the Surface. *Catal. Sci. Techno.* **2015,** *5* (3), 1783-1791.

(36) Hegde, M. S.; Madras, G.; Patil, K. C. Noble Metal Ionic Catalysts. *Acc. Chem. Res.* **2009,** *42*, 704−712.

(37) Kresse. G; Hafner, J. Ab initio Molecular Dynamics for Liquid Metals. *Phys. Rev. B* **1993,** *47* (1), 558-561.

(38) Dudarev, S. L; Botton, G. A.; Savrasov, S. Y.; Humphreys, C. J.; Sutton, A. P. Electron-Energy-Loss Spectra and the Structural Stability of Nickel Oxide: An LSDA1+U Study. *Phys. Rev. B* **1998,** *57*, 1501-1509.

(39) Perdew, J. P.; Burke, K; Ernzerho, M. Generalized Gradient Approximation Made Simple. *Phys. Rev. Lett.* **1996,** *77* (18), 3865-3868.

(40) Walle., A. v. d.; M. Astaa.; G. Cederb. The Alloy Theoretic Automated Toolkit: A User Guide. *Calphad* **2002,** *26* (4), 539-553.

(41) Dubale, A. A.; Pan., C.-J.; Tamirat., A. G.; Chen., H.-M.; Su., W.-N.; Chen., C.-H.; Rick., J.; Ayele., D. W.; Aragaw., B. A.; Lee., J.-F.; Yang., Y.-W.; Hwang., B.-J. Heterostructured Cu_2O/CuO Decorated with Nickel as a Highly Efficient Photocathode for Photoelectrochemical Water Reduction. *J. Mater. Chem. A* **2015,** *3*, 12482–12499.

(42) Naghash., A. R.; Etsell., T. H.; Xu., S. XRD and XPS Study of Cu-Ni Interactions on Reduced Copper-Nickel-Aluminum Oxide Solid Solution Catalysts. *Chem. Mater.* **2006,** *18*, 2480-2488.

(43) Bard., A. J.; Faulkner., L. R., Electrochemical Methods: Fundamentals and Applications. Second Ed. ed.; Wiley, New York: 2009.

(44) Singh, R. P.; Arora, P.; Nellaiappan, S.; Shivakumara, C.; Paliwal, M.; Sharma, S. Electrochemical Insights into Layered La_2CuO_4 Perovskite: Redox Active Ionic Copper for Selective CO_2 Electroreduction. *Electrochim. Acta* **2019,** *326*, 134952-134963.

(45) Sharma, S.; Sravan Kumar, K. B.; Chandnani, Y. M.; Phani Kumar, V. S.; Gangwar, B. P.; Singhal, A.; Deshpande, P. A. Mechanistic Insights into CO2 Methanation over Ru-Substituted CeO_2. *J. Phys. Chem. C* **2016,** *120* (26), 14101-14112.

(46) Cheng, T.; Xiao, H.; Goddard, W. A. Reaction Mechanisms for the Electrochemical Reduction of CO_2 to CO and Formate on the Cu(100) Surface at 298K from Quantum Mechanics Free Energy Calculations with Explicit Water. *J. Am. Chem. Soc.* **2016,** *138*, 13802−13805.

(47) Mishra, A. K.; Roldan, A.; Leeuw, N. H. D. CuO Surfaces and CO_2 Activation: A Dispersion-Corrected DFT+ U Study. *J. Phys. Chem. C* **2016,** *120*, 2198-2214.

(48) Heinemann, M.; Eifert, B.; Heiliger, C. Band Structure and Phase Stability of the Copper Oxides Cu_2O, CuO, and Cu_4O_3. *Phys. Rev. B* **2013,** *87*, 115111-115115.

(49) Ahmad., R.; Singh., A. K. Synergistic Core–shell Interactions Enable Ultra-low Overpotentials for Enhanced CO_2 Electro-reduction Activity. *J. Mater. Chem. A* **2018,** *6*, 21120-21130.

(50) Peterson, A. A.; Abild-Pedersen, F.; Studt, F.; Rossmeisl, J.; Norskov, J. K. How Copper Catalyzes the Electroreduction of Carbon Dioxide into Hydrocarbon Fuels. *Energ. Environ. Sci.* **2010,** *3*, 1311-1315.

(51) Gao, D.; Zhou, H.; Wang, J.; Miao, S.; Yang, F.; Wang, G.; Wang, J.; Bao, X. Size-Dependent Electrocatalytic Reduction of CO_2 over Pd Nanoparticles. *J. Am. Chem. Soc.* **2015,** *137*, 4288-4291.

(52) Ruban., A.; Hammer., B.; Stoltze., P.; Skriver., H. L.; Norskov., J. K. Surface Electronic Structure and Reactivity of Transition and Noble Metals. *J. Mol. Catal. A: Chem.***1997,** *115*, 421-429.

TOC

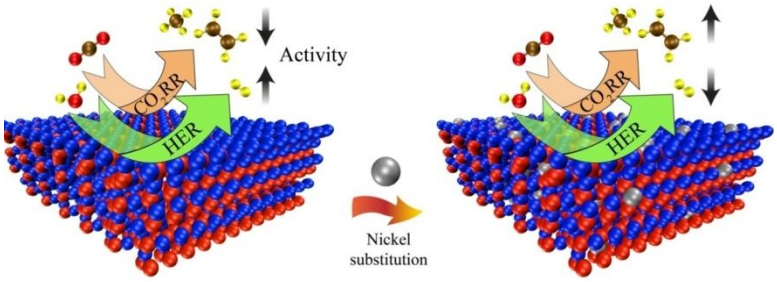

Synopsis: Adopting the substitution chemistry, here, isomorphic atomic substitution of Ni over CuO host improved its redox electrochemistry and selective conversion of CO_2 to hydrocarbons by suppressing HER.

*****